crystals

MDPI

Article

Activated Carbon–Geopolymer Composites: Influence of Particle Size and Content on CO_2 Adsorption and Mechanical and Thermal Properties

Daniela Řimnáčová *, Ivana Perná, Martina Novotná, Monika Šupová, Martina Nováková and Olga Bičáková

Institute of Rock Structure and Mechanics, The Czech Academy of Sciences, V Holešovičkách 94/41, 18209 Prague, Czech Republic; perna@irsm.cas.cz (I.P.); novotna@irsm.cas.cz (M.N.); supova@irsm.cas.cz (M.Š.); novakova@irsm.cas.cz (M.N.); bicakova@irsm.cas.cz (O.B.)

* Correspondence: rimnacova@irsm.cas.cz; Tel.: +420-266009274

Abstract

This study aims to develop and characterize innovative geopolymer composites by incorporating activated carbon into a geopolymer matrix to create a novel, effective sorption material suitable for non-dusty or medium-temperature environmental applications. Specifically, it examines the impact of using a single source of activated carbon, both in its original granular form and milled form, at two different loading levels for each. The research focuses on evaluating how these variations influence the textural, adsorption, mechanical, and thermal properties of the resulting geopolymer composites, with particular attention to strength and thermal stability under operational conditions. The CO_2 adsorption capacity of the composites measured at 25 °C and pressure up to 0.1 MPa varied from 48.8 to 60.0 mg.g^{-1}, with the highest performance observed at a lower content of the granular form, while commercial pure activated carbon reached 120.8 mg.g^{-1}. However, incorporation of a granular form negatively affected thermal stability (approximately 20 wt.% weight loss) and significantly reduced compressive strength (below 45 MPa) due to increased material inhomogeneity. Despite these limitations, both types of composites show promising potential for environmental applications. However, further optimization is required to balance sorption capacity, strength, and thermal stability.

Keywords: activated carbon; geopolymer; adsorption; compressive strength; textural properties; thermal properties

check for updates

Academic Editor: Philippe Trens

Received: 10 September 2025
Revised: 10 October 2025
Accepted: 13 October 2025
Published: 15 October 2025

Citation: Řimnáčová, D.; Perná, I.; Novotná, M.; Šupová, M.; Nováková, M.; Bičáková, O. Activated Carbon–Geopolymer Composites: Influence of Particle Size and Content on CO_2 Adsorption and Mechanical and Thermal Properties. *Crystals* **2025**, *15*, 892. https://doi.org/10.3390/cryst15100892

Copyright: © 2025 by the authors. Licensee MDPI, Basel, Switzerland. This article is an open access article distributed under the terms and conditions of the Creative Commons Attribution (CC BY) license (https://creativecommons.org/licenses/by/4.0/).

1. Introduction

New adsorption materials can be developed and prepared in different ways depending on their possible use and applications, mainly the need to effectively remove pollutants from different environments, such as water, air, or soil. The utilization of stable sorption materials in demanding environments offers significant ecological and economic benefits, which are manifold and stem from enhanced performance, longevity, and efficiency of the materials under challenging conditions.

Porous materials have been shown to effectively capture both organic and inorganic pollutants, demonstrating their potential as efficient adsorption materials [1–4]. The primary mechanism is adsorption occurring on the surfaces of their pores. This process is crucial for capturing and retaining various pollutants, as the porous structure provides a

vast surface area for interaction. The efficiency of adsorption is significantly influenced by the size, distribution, and surface chemistry of the pores.

A favorable pore size distribution, including mesopores, is typical, for instance, in geopolymer materials [5], which are a new type of material that has gained considerable attention in the field of materials science and engineering. Geopolymer materials have been developed since 1979 and have been studied in detail worldwide [6–9]. Their structure is mainly amorphous and is composed of various chemical bonds, including siloxane (Si-O-Si) and aluminate (Al-O-Al) bonds in varying proportions to each other [7,10–12]. Geopolymers are typically formed by combining aluminosilicate precursors, such as metakaolin (primary or waste), slag, fly ash, and natural pozzolans, and alkaline activators (aqueous solution of sodium/potassium/calcium silicates) required for the initiation of the geopolymerization reaction [7,12,13]. The aggregates used, regardless of granulometry, can be primary materials, for example, silica sand [14–16] or secondary/waste materials such as slag, waste rock dust/grit, by-products, or fly ash [17–21].

The specific composition of the geopolymer, and thus its properties, may vary according to the type of aluminosilicate precursor, alkaline activator, and/or aggregates used [8,9,13,16,18]. Geopolymers are known for their exceptional strength, durability, and resistance to extreme temperatures and demanding chemical conditions. Therefore, these materials have the potential to play an important role in sustainable construction and various industrial applications [22–28].

Geopolymer materials can also be prepared in porous form using various foaming approaches, including mechanical or chemical foaming and the use of porogenic agents, both of which create foam-like structures [29–31]. These methods enable not only structural applications but also the development of functional materials [29,32]. In recent years, porous geopolymer composites have gained considerable attention due to their ability to combine the mechanical and chemical stability of the geopolymer matrix with a high specific surface area and open pore structures [29,33]. Particular emphasis has been placed on their potential for water and wastewater treatment, where they have demonstrated both efficiency and long-term chemical stability [34]. Although pure geopolymer materials usually show limited adsorption capacity, their combination with additional sorptive components (such as activated carbon) can markedly enhance their performance [32,34,35].

Geopolymer materials have also been explored as potential porous materials for adsorption [2,36]. The most studied in connection with geopolymers is the adsorption of heavy metals [37] or ammonia [20]. A porous open-cell geopolymer based on industrial wastes (blast furnace slag and municipal wastes) has shown adsorption properties for heavy metal cations and cationic dyes [21,38,39].

However, the adsorption properties of the geopolymer alone are not particularly exceptional. The hopeful way to prepare thermally and mechanically stable materials for adsorption in very demanding environments is the incorporation of raw sorption materials into a geopolymer matrix. In the case of activated carbon–geopolymer composites, the activated carbon component carries a large surface area with numerous micropores and mesopores, which are ideal for trapping small molecules and gases. The geopolymer matrix gives the material structural integrity and increases its resistance to high temperatures and corrosive environments, ensuring that the composite remains effective, even for long-term use. New composites based on activated carbon in a geopolymer could be used to separate and capture water vapor, gaseous pollutants generated during combustion processes, and in environments where small particles of activated carbon would be harmful. The incorporation of activated carbon into geopolymers for stable sorbents was studied by Chen et al. [35], who prepared a high-strength adsorbent with enhanced CO_2 adsorption

capacity. However, tests were only performed with a wood-based activated carbon of uniform particle size.

This article focuses on the development of adsorption materials composed of commercial coconut shell-based activated carbon and a specially designed geopolymer matrix. The primary objective is to create materials suitable for applications in conditions where pure activated carbon may be structurally or thermally limited. The presence of a wide range of pore sizes in raw activated carbon and its incorporation into final products could be negatively or positively affected by the geopolymer matrix or by the form and amount of added activated carbon. Otherwise, the form of additive influences the thermal/mechanical/textural/adsorption properties and has a significant impact on the homogeneity of final materials. For this reason, two different variants of activated carbon (original granular and milled form, 0.5–2.0 mm and <0.7 mm, respectively) were used. The formation of geopolymer bonds and the possible influence of activated carbon were monitored by infrared spectroscopy. Structure, mechanical, thermal, and textural properties were discussed, as well as the sorption properties of the prepared materials. The study provides insight into the trade-off between adsorption capacity and thermal/mechanical stability depending on the form and content of activated carbon.

2. Experimental

2.1. Characterization Methods

The chemical compositions of geopolymer components were analyzed by X-ray fluorescence (XRF) (Spectro IQ, SPECTRO Analytical Instruments GmbH, Kleve, Germany). The target material was palladium, positioned at a 90° angle from the central ray. The instrument focused on a 1 mm × 1 mm area, with a maximum anode dissipation of 50 watts and 10 cfm forced-air cooling. It was equipped with a HOPG Barkla crystal. Sample preparation involved the pressed-pellet method, where 4.0 g of material with a particle size of 15–20 μm was mixed for 10 min with 0.9 g of HWC Hoechst wax (Bedburg-Hau, Germany) as a binding additive. The mixture was then pressed at 80 kN. The X-LabPro version 5.1 software automatically converted the elemental results to their corresponding oxides.

The particle size analysis was performed with a Microtrac Sync 5001 particle size analyzer (Microtrac Inc., Montgomeryville, PA, USA) with a measurement range of 0.02–2800 μm. The device is equipped with three red laser resistors and with a Flowsync module whose function is to deliver a powder sample well-dispersed in a liquid medium to the Microtrac Sync 5001 for further analyses. The samples (50–100 mg) were ultrasound-dispersed in water for 30 s and then transported to the measuring cell. The resulting data is the average of 3 measurements.

Compressive strength was determined on 8 × 8 × 8 mm cubes. The experiment was performed on an Inspekt 100 (Hegewald-Peschke, Nossen, Germany) using PMA 4 (Maytec, Olching, Germany), which was (additionally) modified for the compression experiment and increased loading. The measurements were performed on 7 cubes from each mixture, and the results are the average of the measured values. The force for the strength calculation was subtracted from the maximum of the load–displacement record.

Fourier transform infrared (FTIR) spectra were acquired with an iS50 spectrometer (Nicolet Instrument, Madison, WI, USA) using the attenuated total reflection (ATR) technique with a diamond crystal in the mid spectral range 4000–400 cm^{-1} with a resolution of 4 cm^{-1}, averaging 64 scans. All samples were scanned directly as observed in powder form. The resulting spectra were processed using OMNIC version 9 software. Advanced ATR correction was performed on the spectra, which corrected the wavenumber dependence of the band intensity and slight shifts of intense bands in the ATR spectra.

Complex textural characterization of geopolymer composites includes several methods. Gas physical adsorption or mercury intrusion/extrusion porosimetry were usually used for obtaining the complex texture as volumes and surfaces of pores in defined size ranges and porosity [40–42]. Measurements were usually repeated twice to eliminate differences caused by potential material heterogeneity.

An IGA-100 gravimetric sorption analyzer (Hiden Isochema, Warrington, UK) was used to measure the adsorption of CO_2 on both dry and wetted materials. All samples with particles <0.7 mm were first degassed and evacuated at 105 °C. Subsequently, CO_2 adsorption was measured on dry samples at a temperature of 25 °C. Before the second set of measurements, the samples were wetted at 15 °C under a pressure of 5 mbar, and then, CO_2 adsorption was measured under the same conditions as for the dry samples. The surfaces of micropores (S_m) from their CO_2 adsorption isotherms, where the real adsorption capacity (n) was measured at 25 °C and a pressure of 0.1 MPa, were evaluated. The adsorption isotherms were approximated using the Langmuir model [43]. Micropore parameters and pore size distribution were calculated using the modified Dubinin model and the Dubinin–Medek equation [44,45]. Weight loss obtained directly during preparation due to adsorption was monitored and discussed because the porous materials can capture water and organic volatile compounds in pores, and weight loss seems to be a good parameter for the first estimation of volumes of pores and the adsorption behavior of the material.

A volumetric sorption analyzer (Thermo Fisher Scientific, Waltham, MA, USA) was used for the determination of surface properties of micropores and mesopores (size range from 2.2 to approx. 80 nm) of pre-dried materials with particles <0.2 mm, with the main parameter being specific surface area (S_{BET}). Measurement is based on nitrogen physisorption at 77 K and pressurization to 100 kPa. End evaluation of parameters was conducted using the BET method for relative pressure in the range of 0.05–0.3 [46,47]. The pore size distribution and pore volume were evaluated by the BJH method and the Dubinin-Radushkevich model [48].

PASCAL 140 Evo and PASCAL 440 Evo mercury porosimeters (Thermo Fisher Scientific, Waltham, USA) were used for analyzing meso- and macropores (7 nm–112 μm) on pieces of pre-dried samples of approximately 5 mm in size. The pore size distributions and porosity (P) as the main parameters, volume and surface of meso- and macropores (S_{Hg}) were evaluated using the Washburn method with a contact angle of 140° and mercury surface tension of 0.48 n/m [49]. The measurement is based on the intrusion of mercury into pores under increasing pressure and extrusion under decreasing pressure, where the shape of the curve determines the model for evaluating the pore surfaces [50,51]. The detailed description of the method and evaluation of the parameters used is, e.g., in [52].

The indicative parameter of the adsorption capacity of activated carbon and its derivatives is the iodine number. It was determined for pure input materials (AC, GP matrix), as well as for composites containing 13.8 wt.% AC using standardized methods [53].

The geopolymer composites (finely milled (mg) and 8 × 8 × 8 mm cubes (g)) were also put under thermal loading at a temperature of 500 °C on a SETARAM thermal analyzer (Setaram Setsys Evolution, Caluire-et-Cuire, France) and a Derivatograph MOM (System: Paulik, Paulik-Erday, MOM, Budapest, Hungary), respectively. Thermal tests were conducted in an inert atmosphere of either He (SETARAM thermal analyzer) or N_2 (Derivatograph MOM) with the same inert gas flow rate of 20 mL.min^{-1}. The heating rate was 5 °C.min^{-1} in both devices. The effect of this chosen temperature and the type of activated carbon used as an additive in the geopolymer matrix on the thermal stability of the composites and on the structural changes during thermal heating was also investigated. Heat testing on all samples was performed, and the resulting weight loss was recorded and evaluated by Calisto software v1.38.

Microscopic analyses of pore morphology in the materials and at the GP matrix-AC boundary were conducted using a Quanta 450 scanning electron microscope (SEM) equipped with EDS (energy dispersive spectrometer) silicon drift Si(Li) Apollo detector (FEI, Hillsboro, OR, USA) on a polished section. A detailed SEM image analysis of an image in black-and-white resolution without grayscale was performed to determine the porosity characteristics, total visible porosity, and types of pores and cracks, along with their respective proportions, by calculating the percentage of black [54].

2.2. Materials

The geopolymer (GP) matrix was prepared from clay material L05 (ČLUZ a.s., Nové Strašecí, Czech Republic), and an alkaline activator (SiO_2/K_2O = 1.40, H_2O/K_2O = 12.43), which was made using a solution of potassium silicate 3.0 (Vodní sklo, a.s., Prague, Czech Republic) and potassium hydroxide (KOH; Penta, s.r.o., Prague, Czech Republic). The clay material L05, a partially calcined product manufactured from claystones and washed kaolins, was supplied with guaranteed parameters such as chemical composition, purity, and particle size [55]. As this state was insufficient for our purposes, the material was further calcined in a laboratory oven at 750 °C for 4 h prior to application. The chemical composition before and after thermal treatment, including loss of ignition (LOI), is presented in Table 1. X-ray diffraction (XRD) analysis of the fully calcined clay material L05, used for geopolymer synthesis, indicated a predominantly amorphous structure with minor crystalline components, mainly quartz (SiO_2) and anatase (TiO_2), as well as small amounts of muscovite ($KAl_2(AlSi_3O_{10})(OH)_2$), hematite ($Fe_2O_3$), cristobalite ($SiO_2$), and mullite ($Al(Al_{.83}Si_{1.08}O_{4.85})$) [24].

Table 1. Chemical analysis of clay material L05 before and after thermal treatment (the main oxides in wt.%).

L05	Al_2O_3	SiO_2	CaO	Na_2O	K_2O	MgO	Fe_2O_3	TiO_2	LOI
Before	41.99	50.28	0.14	<0.11	0.59	0.14	1.03	1.52	3.65
After	43.24	50.94	0.79	<0.11	0.59	0.14	1.03	1.52	1.21

Activated carbon (AC) used as an adsorption additive to the geopolymer matrix was commercial granular K835 (Brenntag CR s.r.o., Prague, Czech Republic), made from coconut shells, with a declared particle size range of 0.5–2.5 mm [56]. However, the measured particle size distribution was predominantly between 0.5 and 1.99 mm (D_{50} = 0.99 mm, D_{90} = 1.29 mm), and no particles larger than 2 mm were detected. The material also contained a fraction of particles smaller than 0.5 mm, likely generated by abrasion or breakage during handling and transport.

This material was subsequently milled to a particle size < 0.7 mm (D_{50} = 0.06 mm, D_{90} = 0.21 mm) using a laboratory vibration mill. The particle size distributions of both granular and milled AC, determined by granulometry, are shown in Figure S1.

2.3. Sample Preparation

The two forms of activated carbon added to the geopolymer matrix were therefore: (i) the original granular form (G), and (ii) the milled form (M). The preparation of the geopolymer matrix was described in detail in a previous study [18]. The preparation procedure of the composites was carried out in the following steps: (i) mixing of calcined clay material L05 (25 g) and alkaline activator (25 g) in a laboratory mixer stirrer for 10 min, (ii) addition of activated carbon and homogenization (5 min), (iii) pouring of the geopolymer mass into the mold for 8 × 8 × 8 mm cubes and vibrating to remove unwanted bubbles (2 min), (iv) covering molds with a plastic panel to avoid water evaporation (24 h),

and (v) demolding of the solid samples, followed by storage for 28 days in plastic bags and then exposure to air under laboratory conditions. It was important to remove the resulting gas bubbles by vibration because they would negatively affect the mechanical and sorption properties of the solid composite.

The amount of activated carbon added to the fresh geopolymer matrix was 8 g/4 g per 25 g of dry clay material L05 (13.8 wt.%/7.4 wt.%, respectively). Despite the geopolymer matrix's ability to accommodate a greater volume of the granular form, the decision was made to maintain a lower content for both forms, specifically aligning with the maximum amount suitable for milled activated carbon. This approach ensured comparability of the results across both forms of carbon incorporation. The additive proportions and particle sizes of activated carbon are summarized in Table 2, and the geopolymer composites with the additive are shown in Figure 1, where the samples were sectioned to reveal their internal structure.

Table 2. Content and granularity of activated carbon in geopolymer composite (C); M—milled, G—granular.

Material/Parameter	Activated Carbon Content	Size of Particles
	(wt.%)	(mm)
K836	100	0.5–2.0
CM-13.8	13.8	<0.7
CG-13.8	13.8	0.5–2.0
CM-7.4	7.4	<0.7
CG-7.4	7.4	0.5–2.0

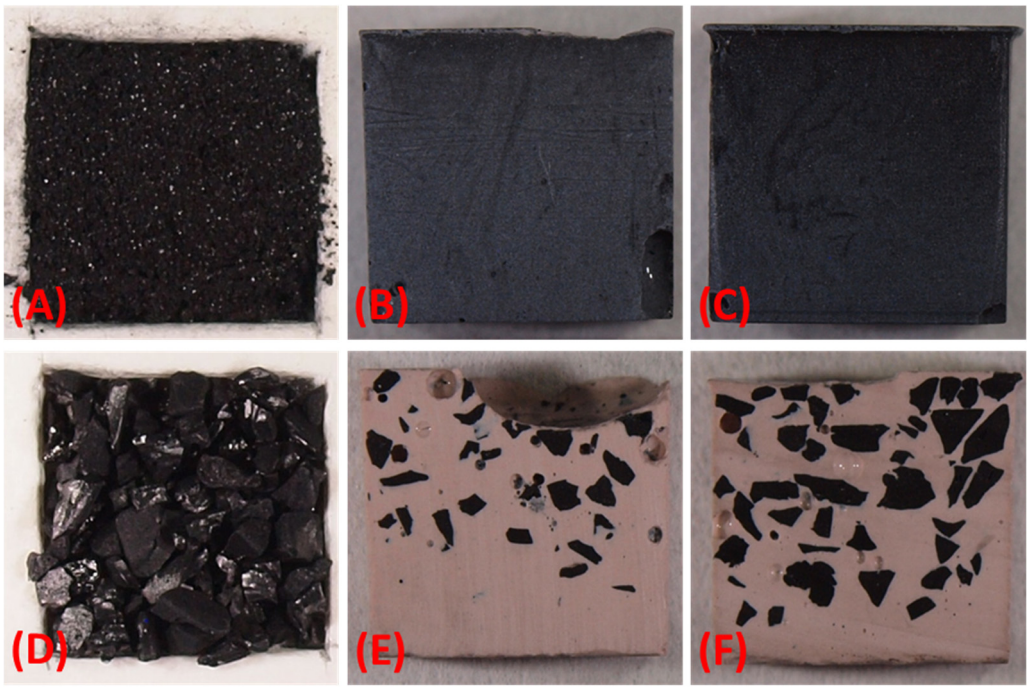


Figure 1. Photos of the cube-shaped samples cut longitudinally for internal structure observation: (**A**) Milled activated carbon; (**B**) CM-7.4, (**C**) CM-13.8, composites with milled activated carbon; (**D**) the raw granular activated carbon; (**E**) CG-7.4, (**F**) CG-13.8, composites with granular activated carbon.

It was observed that the addition of milled activated carbon significantly reduced the workability of geopolymer composites during mixing and casting compared to the pure matrix, due to increased viscosity. A similar effect was previously reported for carbon nanotubes [57]. In contrast, the addition of granular activated carbon in the studied amounts

had no significant impact on the workability. However, as shown in Figure 1E,F, the incorporation of granular AC led to poor homogenization due to the density difference between the AC and the geopolymer matrix. As a result, the lower-density granular particles tended to float toward the upper part of the composite during setting. Although the matrix could accommodate even higher contents of granular activated carbon, comparable contents were selected to enable a direct comparison with the milled form.

3. Results and Discussion

3.1. Verification of Geopolymer Formation

The FTIR spectra of all input materials (active carbon, L05) and GP matrix, and their comparison with geopolymer composites with active carbon, are shown in Figure 2. The spectra of the activated carbon, GP matrix, and the CM and CG series contain a wide peak at 3440 and 3420 cm^{-1}, respectively, associated with the stretching vibrations of OH bonds in water molecules due to the residual water and moisture content in the materials [58]. Another peak corresponding to the bending vibrations of H-O-H bonds is situated at 1640 cm^{-1}, which is evident in the spectra of geopolymer matrices after alkali activation, in both without (GP matrix) and with activated carbon CM and CG series).

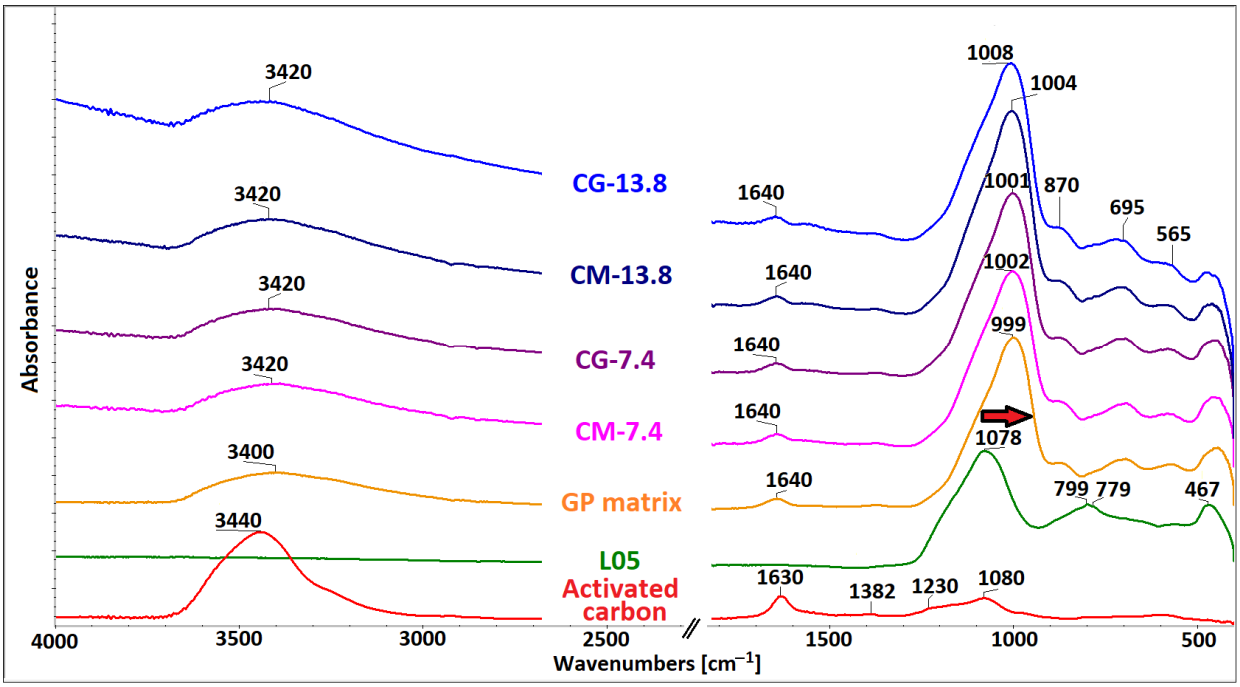


Figure 2. Comparison of ATR-FTIR spectra of original materials (activated carbon, clay material L05, and geopolymer (GP matrix) and geopolymer composites (C) with milled/granular active carbon (M/G). Spectral part 2500–2000 cm^{-1} is not shown because this region contains only diamond crystal noise and carbon dioxide spectral bands.

The most principal band apparent in the spectral region 1300–900 cm^{-1} in the spectra of L05, GP matrix, CG, and CM can be attributed to the asymmetric stretching vibrations (ν3) of Si–O in the SiO_4 tetrahedra and Si–O–Al groups in aluminosilicates [59]. The band near 870 cm^{-1} is a superposition of signals from Si–O bonds. Another band at 450–470 cm^{-1} is ascribed to the bending vibrations (ν4) of Si-O. The weak band in the region 720–840 cm^{-1} is attributed to the Si–O–Si symmetric stretching vibrations of bridging oxygens between tetrahedra [60].

The position of the principal band in the spectra of the metakaolin-based clay material (L05) was seen at 1078 cm^{-1}. The process of alkaline activation and the formation of

a geopolymer structure caused a spectral shift in the principal stretching band, located originally at 1078 cm^{-1} in the L05 spectrum, to lower wavenumbers at 999 cm^{-1} in the spectrum of the GP matrix (see red arrow in Figure 2). This was visible also in other spectra representing geopolymer composites. During this reaction, AlO_4 ions become incorporated into the SiO_4 tetrahedral unit to form a Si-O-Al network structure [61,62]. The formation of the geopolymer structures, i.e., aluminosilicates with long-range structural order, demonstrates the existence of a weak band at ~565 cm^{-1} [63]. The band with more distinctive features at 799 and 779 cm^{-1} relates to quartz [59], which is present in L05 as a minor impurity.

Activated carbon has a well-developed porous structure with several surface functionalities determined by the type, quantity, concentration, and bonding of heteroatoms (phosphorus, sulfur, and oxygen, especially); these are believed to form functional groups such as OH, C=O, P=O, P-O-C, P=OOH, and S=O [64]. One of the dominant absorption bands in the spectrum of activated carbon (red spectrum in Figure 2) appeared at ~1630 cm^{-1} and is attributed to the combined effect of C=C stretching vibrations of the aromatic rings of hydrocarbons and the carbonyl functional group C=O [65]. A weak signal associated with the asymmetric stretching of S=O appeared at ~1382 cm^{-1} [66], while the stretching mode of the P=O, P-O-C, P=OOH bonds was present in the spectral region 1180–1280 cm^{-1} [67]. Since bands S=O and P=O are not very prominent in the activated carbon spectrum, these groups were not too dominant on the activated carbon surface. As was proven by the chemical analysis of the activated carbon analyzed in this study, the total sulfur was bound organically at a concentration of 0.05 wt.%. Another dominant spectral region was a broad band at ~1000–1300 cm^{-1}, commonly found in the spectra of oxidized carbons, and was attributed to stretching of the C-O groups from alcohols, acids, phenols, ethers, and/or ester functional groups [67].

After alkaline activation, the incorporation of activated carbon into the geopolymer material caused a shift in the principal band to higher wavenumbers, i.e., from 999 cm^{-1} (GP matrix) to 1008 cm^{-1} (CG-13.8), so the maximum difference was 9 cm^{-1} (See Figure 2). Changes in wavenumber positions up to 4 cm^{-1} (CM-7.4 and CG-7.4) are within the resolution of the method. Slight shifts of 5 cm^{-1} (CM-13.8) and 9 cm^{-1} (CG-13.8) are insignificant when compared with the shift after the geopolymer reaction of 79 cm^{-1} in the spectrum of the GP matrix (see red arrow in Figure 2). It follows from the above that the addition of activated carbon to the geopolymer matrix caused only a slight spectral shift of the dominant band in the geopolymer composite spectra but did not negatively affect the course of the geopolymer reaction, regardless of the added concentration or granulometry of the activated carbon.

3.2. Characterization of Activated Carbon and Geopolymer Composites

3.2.1. Compressive Strength

The geopolymer composites were also monitored in terms of mechanical properties. For the purpose of testing the material for stability during material handling, transport processes, and adsorption, the compressive strength was investigated. The compressive strength of the samples containing activated carbon after 90 days is presented in Table 3, including standard deviations. Samples containing milled material had higher compressive strength, increasing more with the proportion of additives (see Table 2) than samples with the granular form. A higher proportion of milled additive caused better homogeneity of the material (Figure 1), whereas the opposite trend was found for the granular form (see standard deviations in Table 3).

Table 3. Compressive strength of geopolymer composites with activated carbon.

	Compressive Strength	Standard Deviation
	(MPa)	
GP matrix	72.8	7.5
CM-13.8	105.4	16.4
CG-13.8	40.1	13.1
CM-7.4	62.9	17.9
CG-7.4	37.7	7.3

The addition of milled AC to the geopolymer matrix positively influenced the strength properties. Similar findings were noted for geopolymer materials containing waste stone powders [18]. The study [35] reported that the compressive strength of a similar composite reached 22.3 MPa, while the study [28] showed a compressive strength of 58 MPa for the composite containing 0.5% carbon fibers.

3.2.2. Textural and Adsorption Properties

The textural parameters presented in Table 4, including the specific surface area and volume of micropores, as well as the volume of the meso- and macropores, provide information about pores up to 116 µm in diameter. The variability of the pore surfaces in the materials studied was small for similar samples (see Table S1). Nevertheless, the relationship between parameters n (CO_2 adsorption capacity) and S_m (surface of micropores, Table S1) is evident (R^2 = 0.9638). Thus, the behavioral properties were similar to most solid natural materials [41,68].

Table 4. Textural and sorption parameters.

Sample	Parameter						
	S_{BET}	V_m	V_{Hg}	P_{or}	n	IN	E_{sorp}
	($m^2.g^{-1}$)	($mm^3.g^{-1}$)		(%)	($mg.g^{-1}$)	($mg.g^{-1}$)	($kJ.mol^{-1}$)
GP matrix	120.3	5.7	25.8	4.0	54.4	25	16.9
AC	903.7	21.8	228.5	20.5	120.8	985	10.1
CM-13.8	144.2	4.0	31.4	4.8	48.8	129	13.1
CG-13.8	142.3	7.1	60.3	9.0	53.7	145	13.6
CM-7.4	117.0	4.1	28.7	4.5	55.6	90	15.2
CG-7.4	135.0	7.2	47.9	7.3	60.0	95	15.5

S_{BET}—specific surface area (determined by N_2 adsorption measurements), V_m—volume of micropores (determined by CO_2 adsorption measurements), V_{Hg}—volume of meso- and macropores (determined by mercury porosimetry), P_{or}—porosity, n—real adsorption capacity of CO_2 at 25 °C up to 0.1 MPa, IN—iodine number, E_{sorp}—Adsorption energy.

Meso- and macropores, which strongly influence the stability of materials, were the main contributors to the total volume of pores (Table 4, Figure 3). In contrast, micropore volume plays a key role in adsorption processes in activated carbon, particularly for certain gases, due to the comparable sizes of molecules and pores [69]. The activated carbon had four times higher micropore volume (V_m) and an eightfold higher level of surface area of mesopores (S_{BET} data) than the GP matrix (Table 4). The addition of AC affected the content of pores <6 nm in the composite (Figures S2 and S3). The addition of milled AC to the geopolymer matrix decreased the volume of micropores (V_m) by approximately 28.1 and 29.8% for 4 g and 8 g additions, respectively (see Table 4). In contrast, an enhanced micropore volume (26.3 and 24.6%) was seen following the addition of granular AC (4 g and 8 g, respectively) to the geopolymer matrix (see Table 4 and Figure S2).

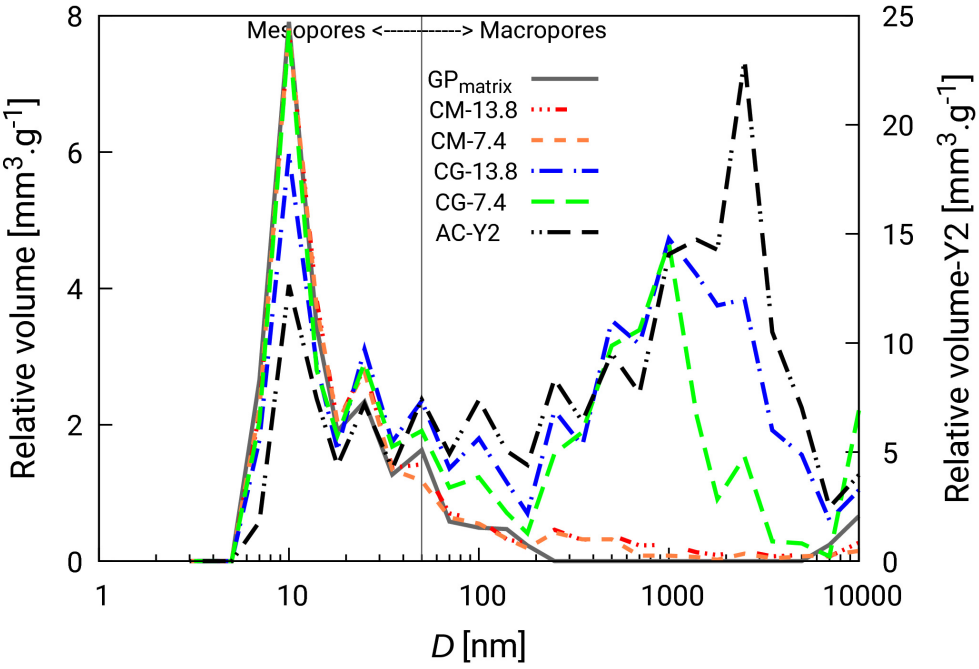


Figure 3. Pore size distribution of samples with added activated carbon and basic mass measured by mercury porosimetry, AC is on the Y2 axis (AC-Y2).

The pore size distribution obtained using mercury porosimetry (Figures 3 and 4) showed clear differences between the granular and milled forms of additives. It is evident that the initial GP matrix had a relatively high volume of pores <250 nm and almost no larger pores. The content of these pores was about eight times lower than in pure activated carbon (Table 4), but the low porosity (*P*) of the GP matrix reflected the fact that the material had a low content of pores >250 nm (Figures 3 and 4), which significantly influences the permeability and surface characteristics. At this point, the question arose as to whether the pore size distribution and porosity of the GP matrix would be affected by the addition of AC. It was found that the addition of milled activated carbon did not significantly affect the textural properties of the composites, and the *P* value was similar to that of the GP matrix. A similar trend was observed in previous work, where the addition of waste stone powders did not significantly affect porosity [18]. In contrast, the incorporation of granular AC into the geopolymer matrix enhanced its pore characteristics by increasing the proportion of pores larger than 250 nm (see Figure 3 and Table 4).

The proportion of pore volumes in defined size classes (Figure 4), N_2 adsorption isotherms (Figure 5), and micropore size distribution (Figure S1) confirm the fact that the materials with the addition of milled activated carbon were microporous (presence of pores <2 nm) and mesoporous (presence of pores 2–50 nm), with the sum of the micro- and mesopore volumes being in the range of 75.3–82.7% (green and red in Figure 4). This had no negative effect on the composition of the GP matrix (85.2%). Conversely, the addition of granular activated carbon, with the sum of micro- and mesopore volumes being between 37.6 and 51.7%, reproduced the properties of AC (25.8%). Total pore volumes of all materials are demonstrated as a line with points in Figure 4. The adsorption–desorption N_2 isotherms (Figure 5) fell into group IV, with the H3 type of hysteresis on the adsorption–desorption curve pointing to the prevailing wedge-shaped pores characteristic of mainly micro-mesoporous materials [42,70,71]. A relatively steep rise at the start of the curve (p/po 0–0.4) indicated monomolecular layer adsorption and a high volume of micropores, followed by multimolecular layer adsorption and capillary condensation (p/po 0.4–0.9). Hysteresis and an S shape point to the presence of mesopores. A wide hysteresis with

inflection points at p/po = 0.4 on the desorption curve indicates the presence of ink-bottle pores. Wedge-shaped pores are more open than the cylindrical pores found, for example, in activated carbon [70,71].

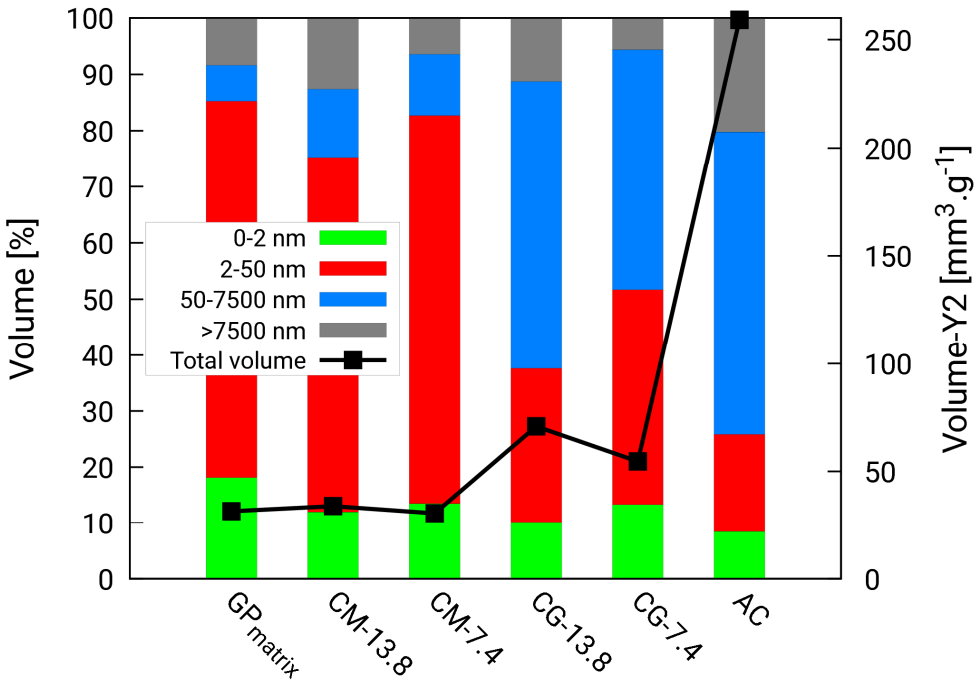


Figure 4. The proportion of volumes in defined pore size classes (bars) and total pore volume (line with points on Y2 axis) obtained by mercury porosimetry. Total volume is the sum of V_m and V_{Hg}.

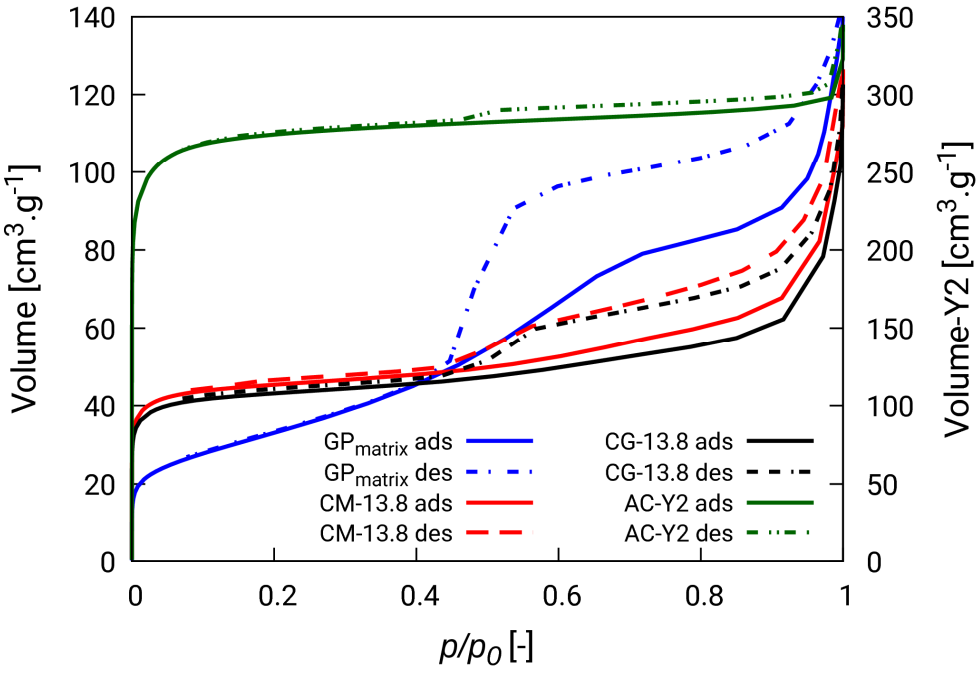


Figure 5. Nitrogen adsorption–desorption isotherms and the amount of N_2 in pores in pressure steps; the four types and courses of the hysteresis loops are shown; AC is on the Y2 axis (AC-Y2).

The gentle rise of adsorption at $p/p_0 < 0.4$ and the small adsorption amount at $p/p_0 > 0.9$ showed that the activated carbon and composites with the granular form had larger volume fractions of macropores (d > 50 nm) and smaller volume fractions of micropores (d < 2 nm).

Generally, in the materials studied, molecules had worse conditions for penetration/catching onto the pore surface and needed to expend higher energy for sorption (Table 4) [46,72]. As can be seen in Table 4 and Table S1, activated carbon had a relatively high porosity and surfaces of pores. The sorption energy of activated carbon was about half as much as that of composites, caused by the easy capture of CO_2 molecules onto carbon surfaces. Prepared composite materials had a twofold lower ability to capture gas (e.g., CO_2, N_2) than commercial activated carbon (Figure 6). Activated carbon, as well as most materials, usually has a lower gas (e.g., CO_2, N_2) adsorption capacity at higher temperatures because the Van der Waals forces between CO_2 or N_2 molecules and the surface of activated carbon weaken with rising temperatures, as confirmed by studies [73,74]. There is evidence for a rapid increase in adsorption and a higher measured adsorption capacity for pure activated carbon (see column n in Table 4), as well as the estimated total adsorption value, determined using the Langmuir equation (n_L = 4.556 mmol.g^{-1}, p_L = 0.07 MPa). Composites exhibited a rapid increase in adsorption at pressures of up to 0.01 MPa due to the availability of free sites for adsorption. This was followed by a slower increase at higher pressures as the adsorption sites gradually became occupied. The Langmuir pressure of composites CM-7.4 and CG-7.4 is lower than 0.01 MPa (p_L are 0.0084 and 0.0067 MPa, respectively), and their higher n_L values are 1.26 and 1.32 mmol.g^{-1}, respectively. In contrast, the CM-13.8 and CG-13.8 composites with a larger amount of additive have higher p_L (0.0195 MPa and 0.0135 MPa) and lower n_L (1.24 mmol.g^{-1} and 1.27 mmol.g^{-1}, respectively). The GP matrix needed a shorter time to establish equilibrium than composites (having a low p_L of 0.56 MPa) with the lowest n_L (GP$_{matrix}$ 1.21 mmol.g^{-1}).

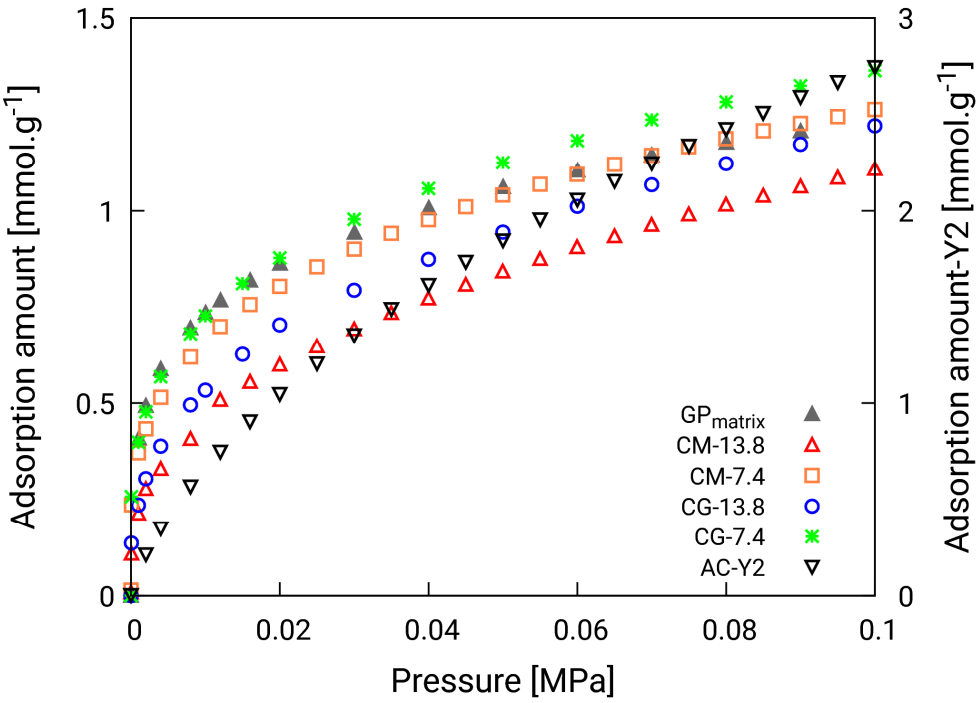


Figure 6. CO_2 adsorption isotherms at 25 °C and pressure to 0.1 MPa; AC is on the Y2 axis (AC-Y2).

Other studies report similar CO_2 adsorption values at 25 °C. In our work, the CG-7.4 sample exhibits a CO_2 adsorption capacity of 1.364 mmol.g^{-1}, compared to the 1.49 mmol.g^{-1} reported for a similar composite in [35]. Incorporation of zeolite can further enhance adsorption, reaching up to 2.6 mmol.g^{-1} at 30 °C, as reported in [75].

The higher adsorption capacity for the larger molecules of the CG composites was also confirmed using the iodine number (see Table 4). The adsorption IN of the pure GP matrix was notably low (25 mg.g^{-1}), whereas the adsorption IN of the CM-13.8 and CG-13.8

composites reached 129 and 145 mg.g^{-1}, respectively. The IN of the CM-7.4 and CG-7.4 was 90 and 95 mg.g^{-1}. IN is closely connected with the content of mesopores.

In experiments with wetted material and CO_2 adsorption, it was observed that the adsorption capacity of activated carbon doubled upon wetting, whereas the GP matrix showed the opposite trend (see Figure 7A). Composites behaved similarly to the GP matrix, showing a decrease in CO_2 adsorption capacity upon wetting. However, this effect was less-pronounced in composites with a higher proportion of AC (Figure 7B,C). Despite this decrease, the adsorption capacity remains sufficient for applications where water vapor is present together with captured gases.

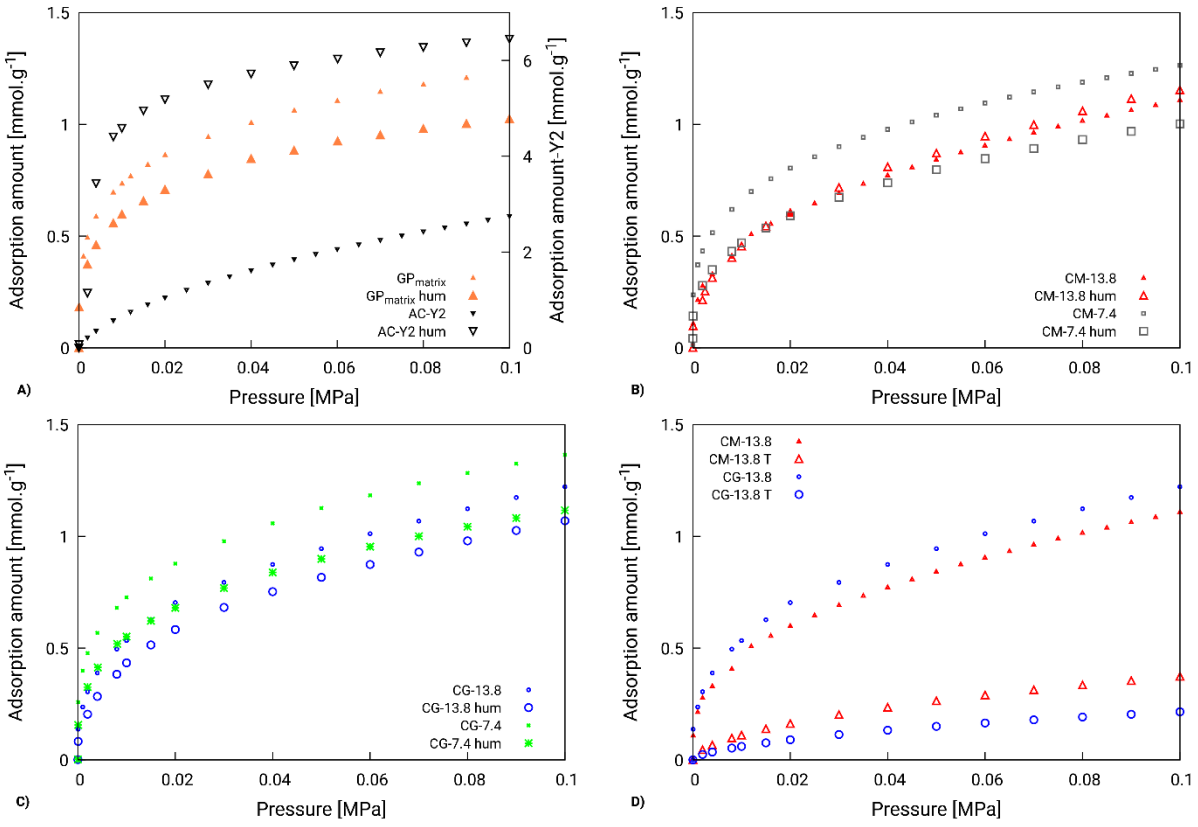


Figure 7. CO_2 adsorption isotherms at 25 °C and pressure 0.1 MPa of (**A**) AC and GP matrix, (**B**) CM composites, (**C**) CG composites without (small points) and after (large points) humidification by water vapor at 25 °C, 5 mbar; AC is on the Y2 axis (AC-Y2); (**D**) composites with higher amount of additive before (small points) and after (large points) thermal degradation analyses.

3.2.3. Thermogravimetric Analyses

All of the prepared materials (geopolymer matrix and geopolymer composites) under controlled heating of up to 500 °C provided us with information on their heat stability. The behaviors of these materials on two different thermogravimetric instruments were compared (Figures S4 and S5). In both cases, changes in weight were recorded and evaluated (Table 5). It has also been verified that adequate results can be obtained under a He atmosphere using the same conditions (cube, heating rate 5 °C.min^{-1}, carrier gas flow rate 20 cm^3.min^{-1}) on the same Derivatograph MOM device. The use of inert atmospheres such as N_2 or He does not show a significant effect on the weight change during heating, as demonstrated in Figure S4. The color changes before and after controlled heating of the cube were also recorded by the camera (Figure 8). It was difficult to achieve homogeneity of the mixture and equal distribution of granular AC particles in the composite when mixing a geopolymer with granular AC. Although heating of the composites prepared in this way was slow and gradual, heat transfer through the cube structure did occur.

The changes resulted in non-uniform cracking of the cube, leading to its total destruction. During heating, the geopolymer gradually released water, both physically bound (up to 100 °C) and chemically bound (up to 300 °C). Water bound in hydroxyl groups is released at temperatures above 300 °C [76]. The AC incorporated in the geopolymer partially retained moisture, as evidenced by the slightly lower weight loss (Table 5 and Figure S5). The accumulation of simple substances and their release from the inside of the cube was responsible for partial or complete destruction due to the increase in pore pressure with increasing temperature. It was found that increasing the temperature and water evaporation had a negative effect on the strength of geopolymers because of the pore pressure increase inside the geopolymer [77].

Table 5. Comparison of the decrease in the weight of the samples (wt.%) as a function of final temperature for a cube (N_2 atmosphere; Δm_{cube}) and a powder sample (He atmosphere; Δm_{powder}).

Sample	Δm_{cube}	Δm_{powder}
	(wt.%)	
GP matrix	12.23	8.05
AC	-	1.95
CM-13.8	19.48	7.80
CG-13.8	20.13	7.76
CM-7.4	15.14	7.98
CG-7.4	19.11	7.91

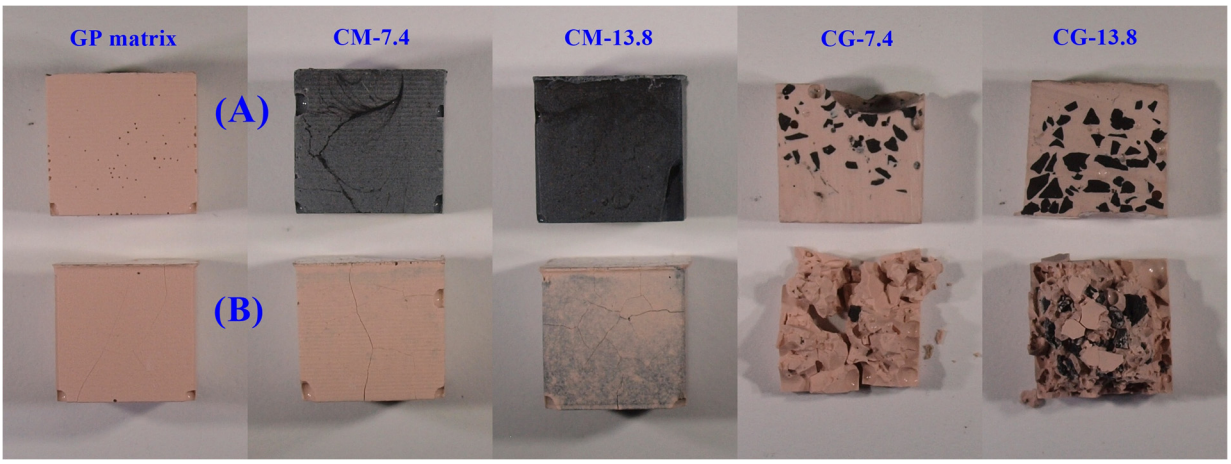


Figure 8. Color changes before (**A**) and after (**B**) heating of the cube from the GP matrix and composites with granular/milled AC.

The heating of activated carbon in powder form was also carried out for comparison. The investigated final temperature of 500 °C had almost no effect on the change in AC behavior (weight loss 1.95 wt.%) (Table 5); the change in weight would only become evident at higher temperatures above 800–900 °C. Activated carbon has the ability to bind moisture contained in the GP matrix in which it was incorporated, as indicated by the lower weight loss in the powdered composites compared to the initial GP matrix. The CO_2 adsorption experiment with samples containing 13.8 wt.% AC demonstrated the textural and adsorption changes in composites after heating. The micropore surface area decreased to 72.0 and 40.1 $m^2.g^{-1}$ for CM-13.8 and CG-13.8, respectively. The micropore volume decreased to 2.5 $mm^3.g^{-1}$ and 1.4 $mm^3.g^{-1}$ for CM-13.8 and CG-13.8, respectively. Similarly, the CO_2 adsorption capacity declined from 1.11 $mmol.g^{-1}$ to 0.373 $mmol.g^{-1}$ for CM-13.8 and from 1.222 to 0.215 for CG-13.8 composites (see isotherms in Figure 7D). The more significant decrease in adsorption capacity of the CG was caused by a stronger

destruction of the composite with added granular activated carbon. The composite CM prepared by mixing finely milled AC into the GP matrix behaved differently. In this case, a well-homogenized mixture was formed ((Figures 1B,C and 8). The latter also showed a color change after thermal heating due to the release of simple volatile substances (Figure 8), but did not show complete degradation compared with the CG composite comprising the granular form of AC. This finding indicates that the composite containing milled AC offers improved usability in medium-temperature cleaning processes compared to the granular form. The incorporation of granular AC into the geopolymer matrix resulted in heterogeneity, which led to reduced thermal stability of the composites. However, the stability of the composites with granular AC can be maintained by keeping the operating temperature below 300 °C in applications such as gas capture.

3.2.4. Microscopic Analyses

The geopolymer composites with 13.8 wt.% of AC before and after heating to 500 °C were analyzed by SEM. The general view of the composite with milled and granular forms and the composites after heating to 500 °C is shown in Figure 9. There, the difference in granulometry of the additive and better homogeneity of the sample with milled activated carbon were evident (Figure 9A,B). Larger bubbles caused by air and water migration during the setting and hardening of geopolymer are more prevalent in CM. However, they cannot be measured by mercury porosimetry because their size exceeds the instrument's detection range. In CG, microcracks are evident as small defects in the matrix near and around AC particles. The destruction of the composites, the AC particles, and the surrounding GP matrix occurred after heating the cube blocks to 500 °C. This phenomenon was more obvious in the composite with the incorporated granular form of AC, where cracks and defects occur around unreacted AC particles (Figure 9C,D).

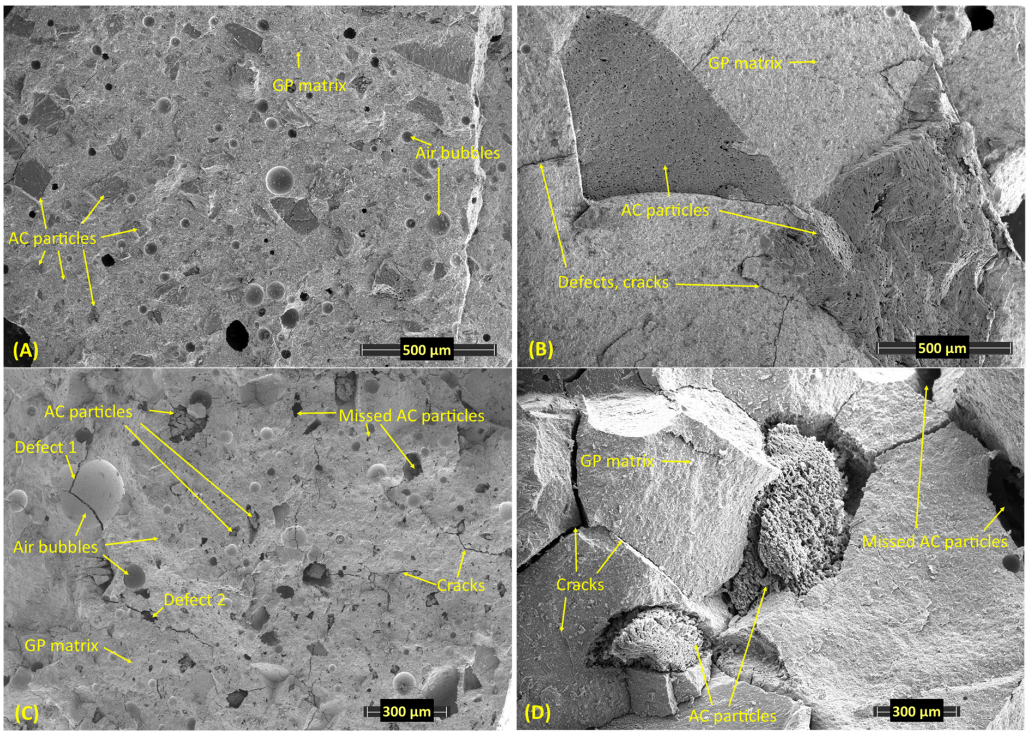


Figure 9. (**A**) CM composite, the scale 500 µm, (**B**) CG composite, the scale 500 µm, (**C**) CM composite after heating to 500 °C, the scale 300 µm, (**D**) CG composite after heating to 500 °C, the scale 300 µm; magnification 200x.

A detailed image analysis (Figure S6A–D) confirms that the composites become more porous after heating compared to their pre-heated state. More pronounced damage was

observed in the CG composite, with the porosity increasing from 1.5% to 3.9%, while the CM composites exhibited imperceptible changes, with the porosity rising slightly from 1.1% to 1.4%. The porosity values obtained through image analysis were lower than those measured by mercury porosimetry due to the limited resolution of image analysis for detecting pores smaller than 25 nm. On the other hand, the pores and cracks larger than 116 µm are visible by this method, e.g., an aperture longer than 300 µm after the disintegration of an AC particle on the right of Figure 9D and Figure S6D.

The low content of larger pores in the milled form of the additive showed that a significant portion of the pores were opened at the geopolymer–AC boundary. Therefore, some pores were partially clogged with geopolymer and deformed due to the pressure exerted during the maturation of the GP matrix (Figure 10A,B). This fact is confirmed by the size distribution of pores obtained by mercury porosimetry, where pores < 50 nm dominate in the CM samples (Figures 3 and 4, Table 4). The thermal process led to the release of moisture and geopolymer matrix from the pores of AC particles in the CM composites, as shown in Figure S7. Pore filling by the matrix (other type) was also observed in a study [78]. On the other hand, the CG sample (Figure 10C,D) contains a large content of unfilled pores of various sizes, as shown in Table 4, Figures 3 and 4. The destruction of the pore network after heating to 500 °C in N_2 atmosphere is illustrated in detail in Figure S8, and the creation of new formations at the grain boundary of the AC and GP matrix after heating to 500 °C is shown in Figure S9.

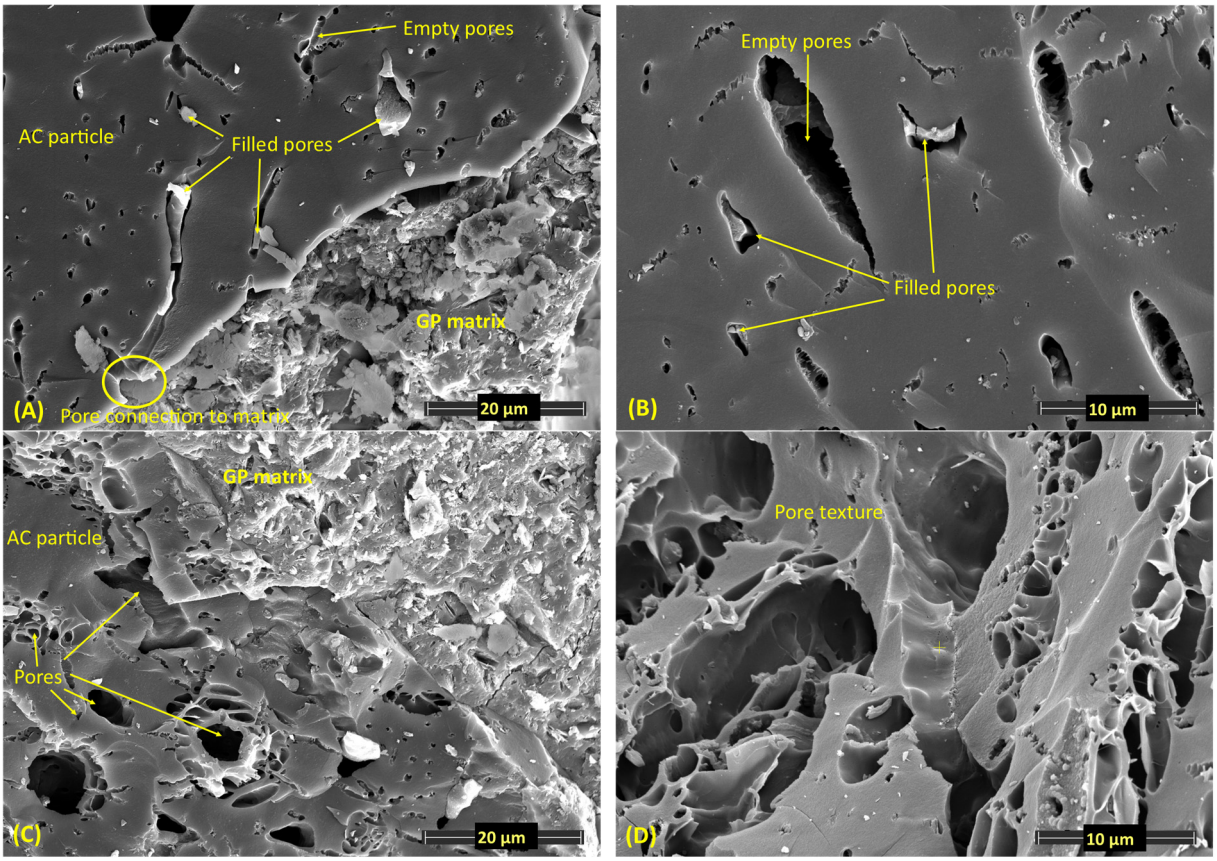


Figure 10. SEM view of the surface of composite (**A**) CM composite, the scale 20 µm, (**B**) AC particle in detail in CM composite, the scale 10 µm, (**C**) CG composite, the scale 20 µm, (**D**) AC particle in detail in CG composite, the scale 10 µm; magnification 5000×/10,000×.

Geopolymers have proven to be effective matrices for incorporating activated carbon in cleaning-related applications, providing adequate mechanical integrity and environmental stability. Although the pore spaces of both milled and granular activated carbon are

partially blocked by the matrix, the resulting composites maintain satisfactory adsorption capacity. In the case of milled AC, the content is limited to approximately 13.8 wt.% due to reduced workability, while the use of granular AC allows for higher loadings without compromising processing. However, composites containing granular AC are more suitable for processes up to 300 °C, such as gas cleaning or air filtration, due to their reduced thermal stability at elevated temperatures.

4. Conclusions

The main findings of the presented results can be summarized as follows:

- Activated carbon K835 was successfully used as an additive in the preparation of geopolymer composites. The resulting materials were solid, mechanically resistant, and insoluble in water;
- FTIR analysis confirmed that the addition of activated carbon to the geopolymer matrix did not negatively affect the geopolymerization process, regardless of the added concentration or granulometry of activated carbon;
- The mechanical properties of the composites remained comparable to the pure geopolymer matrix, indicating that activated carbon does not compromise structural integrity;
- The incorporation of both milled and granular forms of activated carbon enhanced the adsorption capacity of the composites, with the granular form showing superior performance due to better preservation of pore openness;
- Activated carbon significantly influenced the textural properties of the composites, including pore volumes and surfaces and micropore content. The addition of granular form slightly increased total porosity and adsorption capacity;
- The addition of a granular form caused structural inhomogeneity, which led to earlier thermal degradation of the composite at around 500 °C, unlike the milled form, which showed greater thermal resilience;
- CO_2 adsorption experiments revealed that the composites achieved capacities ranging from 48.8 to 60.0 mg.g^{-1} at 25 °C and up to 0.1 MPa, with the highest value observed for the lower content of granular form of activated carbon. For comparison, commercial pure activated carbon reached a CO_2 adsorption capacity of 120.8 mg.g^{-1};
- Despite the reduced thermal stability and compressive strength in composites with granular activated carbon, both types of composites show promising potential for environmental applications, such as gas and pollutant capture, especially under medium-temperature and mechanically demanding conditions.

In conclusion, the study demonstrates that geopolymers are suitable matrices for the development of new adsorption materials. By incorporating activated carbon, it is possible to tailor composites for specific environmental uses, balancing sorption performance with mechanical and thermal stability. These materials offer a viable solution for pollutant capture in demanding conditions, particularly at operating temperatures up to 300 °C. Future research should focus on optimizing the form and content of activated carbon to further improve long-term performance and broaden the range of possible applications.

Supplementary Materials: The following supporting information can be downloaded at https://www.mdpi.com/article/10.3390/cryst15100892/s1, Table S1: Surface parameters; Figure S1: Particle size distribution of activated carbon in original granular (red; part in the background) and milled (blue) form; Figure S2: Micropore size distribution obtained by CO_2 adsorption at 25 °C using modified Dubinin and Dubinin—Medek equations; AC is on the Y2 axis (AC-Y2); Figure S3: Mesopore size distribution obtained by N_2 adsorption at 77 K; BJH method and Dubinin—Radushkevich model; Figure S4: Progress of the change in weight loss (%) in cube samples heated to a temperature of 500 °C in N_2 and He (for two samples) atmosphere at a flow rate of 20 mL.min^{-1}; Figure S5: Progress of the

change in weight loss (wt.%) in the powder samples heated to 500 °C in He atmosphere at a flow rate of 20 mL.min^{-1}; AC is on the Y2 axis (AC-Y2); Figure S6: Detailed image analysis of composites from Figure 9. (A) CM composite (porosity 1.1%), the scale 500 µm; (B) CG composite (porosity 1.5%), the scale 500 µm; (C) CM composite after heating to 500 °C (porosity 1.4%), the scale 300 µm; (D) CG composite after heating to 500 °C (porosity 3.9%), the scale 300 µm; magnification 200×; Figure S7: The release of the geopolymer filling and moisture from the pores of AC particles in a CM composite after thermal treatment at 500 °C in N_2 atmosphere; magnification 10,000×; Figure S8: Example of pore structure destruction in an AC particle embedded in the CG composite after heating to 500 °C in N_2 atmosphere. The image demonstrates the typical collapse and deformation of pores resulting from temperature-induced degradation; magnification 10,000×; Figure S9: An example of temperature-induced transformation is the formation of crystalline form of potassium aluminosilicate at the grain boundary between the AC and GP matrix after heating to 500 °C in N_2 atmosphere; magnification 10,000×.

Author Contributions: Conceptualization, D.Ř.; methodology, D.Ř., M.Š. and O.B.; software, D.Ř. and M.Š.; validation, formal analysis, D.Ř., I.P., M.N. (Martina Novotná), M.Š., M.N. (Martina Nováková) and O.B.; investigation, D.Ř. and O.B.; resources, D.Ř., I.P. and O.B.; data curation, D.Ř., I.P. and M.N. (Martina Nováková); writing—original draft preparation, D.Ř., I.P. and O.B.; writing—review and editing, D.Ř., I.P., M.Š. and O.B.; visualization, D.Ř. and O.B.; supervision, project administration, D.Ř., I.P. and O.B.; funding acquisition, D.Ř., I.P. and O.B. All authors have read and agreed to the published version of the manuscript.

Funding: This research was funded by The Czech Academy of Science, grant number 67985891, The Czech Academy of Science, grant number VP27, and The Czech Academy of Science, grant number VP23.

Data Availability Statement: The original contributions presented in this study are included in the article/Supplementary Material. Further inquiries can be directed to the corresponding author.

Acknowledgments: This work was carried out thanks to the support of the long-term project for the conceptual development of the research organization No. 67985891, and the Strategy AV21 Research Program of the Czech Academy of Sciences, within the framework of the Sustainable Energy VP27 and City as a Laboratory of Change; Construction, Historical Heritage and Place for Safe and Quality Life VP23 research programs. The authors thank Martin Černý for the measurement of mechanical properties.

Conflicts of Interest: The authors declare no conflicts of interest.

References

1. Bouna, L.; Ait El Fakir, A.; Benlhachemi, A.; Draoui, K.; Ezahri, M.; Bakiz, B.; Villain, S.; Guinneton, F.; Elalem, N. Synthesis and Characterization of Mesoporous Geopolymer Based on Moroccan Kaolinite Rich Clay. *Appl. Clay Sci.* **2020**, *196*, 105764. [CrossRef]
2. Ghani, U.; Hussain, S.; Noor-ul-Amin, M.I.; Imtiaz, M.; Ali Khan, S. Laterite Clay-Based Geopolymer as a Potential Adsorbent for the Heavy Metals Removal from Aqueous Solutions. *J. Saudi Chem. Soc.* **2020**, *24*, 874–884. [CrossRef]
3. Strnadová, N.; Matějková, D. Adsorption of Copper and Zinc from Aqueous Solution on $Mg(OH)_2$. *Chem. List.* **2006**, *100*, 803–808.
4. Řimnáčová, D.; Bičáková, O.; Moško, J.; Straka, P.; Čimová, N. The Effect of Carbonization Temperature on Textural Properties of Sewage Sludge-Derived Biochars as Potential Adsorbents. *J. Environ. Manag.* **2024**, *359*, 120947. [CrossRef] [PubMed]
5. Minelli, M.; Medri, V.; Papa, E.; Miccio, F.; Landi, E.; Doghieri, F. Geopolymers as Solid Adsorbent for CO_2 Capture. *Chem. Eng. Sci.* **2016**, *148*, 267–274. [CrossRef]
6. Liew, Y.M.; Heah, C.Y.; Mohd Mustafa, A.B.; Kamarudin, H. Structure and Properties of Clay-Based Geopolymer Cements: A Review. *Prog. Mater. Sci.* **2016**, *83*, 595–629. [CrossRef]
7. Rashad, A.M. Alkali-Activated Metakaolin: A Short Guide for Civil Engineer-An Overview. *Constr. Build. Mater.* **2013**, *41*, 751–765. [CrossRef]
8. Zhang, P.; Zheng, Y.; Wang, K.; Zhang, J. A Review on Properties of Fresh and Hardened Geopolymer Mortar. *Compos. Part B Eng.* **2018**, *152*, 79–95. [CrossRef]

9. Zhang, P.; Gao, Z.; Wang, J.; Guo, J.; Hu, S.; Ling, Y. Properties of Fresh and Hardened Fly Ash/Slag Based Geopolymer Concrete: A Review. *J. Clean. Prod.* **2020**, *270*, 122389. [CrossRef]
10. Amran, Y.H.M.; Alyousef, R.; Alabduljabbar, H.; El-Zeadani, M. Clean Production and Properties of Geopolymer Concrete; A Review. *J. Clean. Prod.* **2020**, *251*, 119679. [CrossRef]
11. Singh, N.B.; Middendorf, B. Geopolymers as an Alternative to Portland Cement: An Overview. *Constr. Build. Mater.* **2020**, *237*, 117455. [CrossRef]
12. Xu, H.; Van Deventer, J.S.J. The Geopolymerisation of Alumino-Silicate Minerals. *Int. J. Miner. Process.* **2000**, *59*, 247–266. [CrossRef]
13. Hanzlíček, T.; Perná, I.; Uličná, K.; Římal, V.; Štěpánková, H. The Evaluation of Clay Suitability for Geopolymer Technology. *Minerals* **2020**, *10*, 852. [CrossRef]
14. Lyu, X.; Robinson, N.; Elchalakani, M.; Johns, M.L.; Dong, M.; Nie, S. Sea Sand Seawater Geopolymer Concrete. *J. Build. Eng.* **2022**, *50*, 104141. [CrossRef]
15. Perná, I.; Hanzlíček, T.; Straka, P.; Steinerová, M. Acoustic Absorption of Geopolymer/Sand Mixture. *Ceram. Silikáty* **2009**, *53*, 48–51.
16. Sui, J.; Li, X.; Zhang, H.; Xu, F.; Deng, J.; Hu, R.; Chen, M. Effect of Different Fibers on Shrinkage Properties and Bonding Properties of Geopolymer Mortar Repair Materials and Analysis of the Mechanism. *Coatings* **2023**, *13*, 1542. [CrossRef]
17. Novotná, M.; Perná, I.; Hanzlíček, T. Review of Possible Fillers and Additives for Geopolymer Materials. *Waste Forum* **2020**, *2*, 78–89.
18. Perná, I.; Novotná, M.; Řimnáčová, D.; Šupová, M. New Metakaolin-Based Geopolymers with the Addition of Different Types of Waste Stone Powder. *Crystals* **2021**, *11*, 983. [CrossRef]
19. Perná, I.; Hanzlíček, T. The Solidification of Aluminum Production Waste in Geopolymer Matrix. *J. Clean. Prod.* **2014**, *84*, 657–662. [CrossRef]
20. Wojtacha-Rychter, K.; Cempa, M.; Król, M.; Kiełbasa, K.; Zhang, L.; Liu, R.; Smolinski, A. A Modified Fly Ash-Based Geopolymer as a Sustainable Solution for Ammonia Storage by Sorption. *Ind. Crops Prod.* **2025**, *230*, 121057. [CrossRef]
21. Karoui, O.; Andrejkovičová, S.; Pato, P.; Patinha, C.; Řimnáčová, D.; Perná, I.; Hajjaji, W.; Rocha, F.; Mlayah, A. Foamed Phosphate By-Product Based Geopolymers and Dye Adsorption Efficiency. *Appl. Clay Sci.* **2024**, *257*, 107446. [CrossRef]
22. Perná, I.; Hanzlíček, T.; Boura, P.; Lučaník, A. The Manufacture of the Grinding Wheels Based on the Ca–K Geopolymer Matrix. *Mater. Manuf. Process.* **2016**, *31*, 667–672. [CrossRef]
23. Perná, I.; Hanzlíček, T.; Lučaník, A.; Šupová, M. Geopolymer-Based Grinding Stones Utilizable in Metal Machining. *Constr. Build. Mater.* **2023**, *363*, 129869. [CrossRef]
24. Perná, I.; Novotná, M.; Hanzlíček, T.; Šupová, M.; Řimnáčová, D. Metakaolin-Based Geopolymer Formation and Properties: The Influence of the Maturation Period and Environment (Air, Demineralized and Sea Water). *J. Ind. Eng. Chem.* **2024**, *134*, 415–424. [CrossRef]
25. Wasim, M.; Ngo, T.D.; Law, D. A State-of-the-Art Review on the Durability of Geopolymer Concrete for Sustainable Structures and Infrastructure. *Constr. Build. Mater.* **2021**, *291*, 123381. [CrossRef]
26. Almutairi, A.L.; Tayeh, B.A.; Adesina, A.; Isleem, H.F.; Zeyad, A.M. Potential Applications of Geopolymer Concrete in Construction: A Review. *Case Stud. Constr. Mater.* **2021**, *15*, e00733. [CrossRef]
27. Hager, I.; Sitarz, M.; Mróz, K. Fly-Ash Based Geopolymer Mortar for High-Temperature Application—Effect of Slag Addition. *J. Clean. Prod.* **2021**, *316*, 128168. [CrossRef]
28. Růžek, V.; Dostayeva, A.M.; Walter, J.; Grab, T.; Korniejenko, K. Carbon Fiber-Reinforced Geopolymer Composites: A Review. *Fibers* **2023**, *11*, 17. [CrossRef]
29. Zhang, X.; Bai, C.; Qiao, Y.; Wang, X.; Jia, D.; Li, H.; Colombo, P. Porous Geopolymer Composites: A Review. *Compos. Part A Appl. Sci. Manuf.* **2021**, *150*, 106629. [CrossRef]
30. Hajimohammadi, A.; Ngo, T.; Mendis, P.; Sanjayan, J. Regulating the Chemical Foaming Reaction to Control the Porosity of Geopolymer Foams. *Mater. Des.* **2017**, *120*, 255–265. [CrossRef]
31. Bai, C.; Shao, J.; Li, X.; Zhang, Z.; Qiao, Y.; Hao, J.; Li, H.; Zheng, T.; Colombo, P. Fabrication and Properties of Slag-Based Geopolymer Syntactic Foams Containing Hollow Glass Microspheres. *Mater. Lett.* **2022**, *308*, 131158. [CrossRef]
32. Yu, H.; Xu, M.; Chen, C.; He, Y.; Cui, X. A Review on the Porous Geopolymer Preparation for Structural and Functional Materials Applications. *Int. J. Appl. Ceram. Technol.* **2022**, *19*, 1793–1813. [CrossRef]
33. Zhang, Z.; Provis, J.L.; Reid, A.; Wang, H. Geopolymer Foam Concrete: An Emerging Material for Sustainable Construction. *Constr. Build. Mater.* **2014**, *56*, 113–127. [CrossRef]
34. Luhar, I.; Luhar, S.; Abdullah, M.M.A.B.; Razak, R.A.; Vizureanu, P.; Sandu, A.V.; Matasaru, P.-D. A State-of-the-Art Review on Innovative Geopolymer Composites Designed for Water and Wastewater Treatment. *Materials* **2021**, *14*, 7456. [CrossRef] [PubMed]

35. Chen, H.; Zhang, Y.J.; He, P.Y.; Liu, L.C. Synthesis, Characterization, and Selective CO2 Capture Performance of a New Type of Activated Carbon-Geopolymer Composite Adsorbent. *J. Clean. Prod.* **2021**, *325*, 129271. [CrossRef]
36. Rasaki, S.A.; Bingxue, Z.; Guarecuco, R.; Thomas, T.; Minghui, Y. Geopolymer for Use in Heavy Metals Adsorption, and Advanced Oxidative Processes: A Critical Review. *J. Clean. Prod.* **2019**, *213*, 42–58. [CrossRef]
37. Ariffin, N.; Mustafa, M.; Bakri, A.; Remy, M.; Mohd, R.; Zaino, A.; Murshed, M.F.; Faris, M.A. Review on Adsorption of Heavy Metal in Wastewater by Using Geopolymer. In *MATEC Web of Conferences*; EDP Sciences: Les Ulis, France, 2017; Volume 97, p. 01023.
38. Ji, Z.; Su, L.; Pei, Y. Characterization and Adsorption Performance of Waste-Based Porous Open-Cell Geopolymer with One-Pot Preparation. *Ceram. Int.* **2021**, *47*, 12153–12162. [CrossRef]
39. Medri, V.; Papa, E.; Mor, M.; Vaccari, A.; Natali Murri, A.; Piotte, L.; Melandri, C.; Landi, E. Mechanical Strength and Cationic Dye Adsorption Ability of Metakaolin-Based Geopolymer Spheres. *Appl. Clay Sci.* **2020**, *193*, 105678. [CrossRef]
40. Dąbrowski, A. Adsorption—From Theory to Practice. *Adv. Colloid Interface Sci.* **2001**, *93*, 135–224. [CrossRef]
41. Římnáčová, D.; Malhocká, A.; Havelcová, M.; Hendrych, J.; Weishauptová, Z. Physicochemical Characteristics of Natural and Anthropogenic Inorganic and Organic Solid Porous Materials: Comprehensive View. *Materialia* **2024**, *33*, 101973. [CrossRef]
42. Thommes, M.; Kaneko, K.; Neimark, A.V.; Olivier, J.P.; Rodriguez-Reinoso, F.; Rouquerol, J.; Sing, K.S.W. Physisorption of Gases, with Special Reference to the Evaluation of Surface Area and Pore Size Distribution (IUPAC Technical Report). *Pure Appl. Chem.* **2015**, *87*, 1051–1069. [CrossRef]
43. Garnier, C.; Finqueneisel, G.; Zimny, T.; Pokryszka, Z.; Lafortune, S.; Défossez, P.D.C.; Gaucher, E.C. Selection of Coals of Different Maturities for CO2 Storage by Modelling of CH_4 and CO_2 Adsorption Isotherms. *Int. J. Coal Geol.* **2011**, *87*, 80–86. [CrossRef]
44. Dubinin, M. Adsorption in Micropores. *J. Colloid Interface Sci.* **1967**, *23*, 487–499. [CrossRef]
45. Medek, J. Possibility of Micropore Analysis of Coal and Coke from the Carbon Dioxide Isotherm. *Fuel* **1977**, *56*, 131–133. [CrossRef]
46. Brunauer, S.; Emmett, P.H.; Teller, E. Adsorption of Gases in Multimolecular Layers. *J. Am. Chem. Soc.* **1938**, *60*, 309–319. [CrossRef]
47. Thommes, M. Physical Adsorption Characterization of Nanoporous Materials. *Chem. Ing. Tech.* **2010**, *82*, 1059–1073. [CrossRef]
48. Dubinin, M.M.; Radushkevich, L.V. Equation of the Characteristic Curve of Activated Charcoal. *Proc. Acad. Sci. USSR Phys. Chem. Sect.* **1947**, *55*, 331–333.
49. Washburn, E.W. The Dynamics of Capillary Flow. *Phys. Rev.* **1921**, *17*, 273–283. [CrossRef]
50. Bernabé, Y.; Maineult, A. Physics of Porous Media: Fluid Flow Through Porous Media. In *Treatise on Geophysics*; Elsevier: Amsterdam, The Netherlands, 2015; Volume 11, pp. 19–41.
51. Scheidegger, A.E. The Physics of Flow Through Porous Media. *Soil Sci.* **1958**, *86*, 355. [CrossRef]
52. Košek, F.; Dudák, J.; Tymlová, V.; Žemlička, J.; Římnáčová, D.; Jehlička, J. Evaluation of Pore-Fracture Microstructure of Gypsum Rock Fragments Using Micro-CT. *Micron* **2024**, *181*, 103633. [CrossRef]
53. *ASTM D4607-14(2021)*; Standard Test Method for Determination of Iodine Number of Activated Carbon. ASTM International: West Conshohocken, PA, USA, 2021. Available online: https://www.astm.org/d4607-14r21.html (accessed on 20 March 2023).
54. Ehrlich, R.; Crabtree, S.J.; Horkowitz, K.O.; Horkowitz, J.P. Petrography and Reservoir Physics I: Objective Classification of Reservoir Porosity (1). *Am. Assoc. Pet. Geol. Bull.* **1991**, *75*, 1547–1562. [CrossRef]
55. České Lupkové Závody, A.S. Mefisto L05. Available online: https://www.cluz.cz/en/metakaolin-general-information (accessed on 12 October 2025).
56. Chemap K835. Available online: http://www.chemap.cz/silcarbon-k835/ (accessed on 12 October 2025).
57. Su, Z.; Hou, W.; Sun, Z. Recent Advances in Carbon Nanotube-Geopolymer Composite. *Constr. Build. Mater.* **2020**, *252*, 118940. [CrossRef]
58. Zheng, J.; Li, X.; Bai, C.; Zheng, K.; Wang, X.; Sun, G.; Zheng, T.; Zhang, X.; Colombo, P. Rapid Fabrication of Porous Metakaolin-Based Geopolymer via Microwave Foaming. *Appl. Clay Sci.* **2024**, *249*, 107238. [CrossRef]
59. Torres-Carrasco, M.; Palomo, J.G.; Puertas, F. Sodium Silicate Solutions from Dissolution of Glasswastes. Statistical Analysis. *Mater. Constr.* **2014**, *64*, 05213. [CrossRef]
60. ElBatal, H.A.; Hassaan, M.Y.; Fanny, M.A.; Ibrahim, M.M. Optical and FT Infrared Absorption Spectra of Soda Lime Silicate Glasses Containing Nano Fe_2O_3 and Effects of Gamma Irradiation. *Silicon* **2017**, *9*, 511–517. [CrossRef]
61. Lee, W.K.W.; Van Deventer, J.S.J. Use of Infrared Spectroscopy to Study Geopolymerization of Heterogeneous Amorphous Aluminosilicates. *Langmuir* **2003**, *19*, 8726–8734. [CrossRef]
62. Rees, C.A.; Provis, J.L.; Lukey, G.C.; Van Deventer, J.S.J. Attenuated Total Reflectance Fourier Transform Infrared Analysis of Fly Ash Geopolymer Gel Aging. *Langmuir* **2007**, *23*, 8170–8179. [CrossRef]
63. Sitarz, M.; Mozgawa, W.; Handke, M. Vibrational Spectra of Complex Ring Silicate Anions—Method of Recognition. *J. Mol. Struct.* **1997**, *404*, 193–197. [CrossRef]
64. Jankowska, H.; Świątkowski, A.; Choma, J. *Active Carbon*; Kemp, T.J., Horwood, E., Eds.; Cornell University: Ithaca, NY, USA, 1991; ISBN 9780130049124.

65. Biniak, S.; Szymański, G.; Siedlewski, J.; Światkoski, A. The Characterization of Activated Carbons with Oxygen and Nitrogen Surface Groups. *Carbon N. Y.* **1997**, *35*, 1799–1810. [CrossRef]
66. Terzyk, A.P.; Rychlicki, G. The Influence of Activated Carbon Surface Chemical Composition on the Adsorption of Acetaminophen (Paracetamol) in Vitro: The Temperature Dependence of Adsorption at the Neutral PH. *Colloids Surf. A Physicochem. Eng. Asp.* **2000**, *163*, 135–150. [CrossRef]
67. Puziy, A.M.; Poddubnaya, O.I.; Martínez-Alonso, A.; Suárez-García, F.; Tascón, J.M.D. Synthetic Carbons Activated with Phosphoric—Acid I. Surface Chemistry and Ion Binding Properties. *Carbon N. Y.* **2002**, *40*, 1493–1505. [CrossRef]
68. Chouikhi, N.; Cecilia, J.A.; Vilarrasa-García, E.; Besghaier, S.; Chlendi, M.; Duro, F.I.F.; Castellon, E.R.; Bagane, M. CO_2 Adsorption of Materials Synthesized from Clay Minerals: A Review. *Minerals* **2019**, *9*, 514. [CrossRef]
69. Allen, T.; Burevski, D. Adsorption of Gases on Microporous Carbons. *Powder Technol.* **1977**, *18*, 139–148. [CrossRef]
70. Li, Z.; Liu, D.; Cai, Y.; Wang, Y.; Teng, J. Adsorption Pore Structure and Its Fractal Characteristics of Coals by N2 Adsorption/Desorption and FESEM Image Analyses. *Fuel* **2019**, *257*, 116031. [CrossRef]
71. Everett, D.H. International Union of Pure and Applied Chemistry (IUPAC) Manuals of Symbols and Terminology for Physico Chemical Quantities and Units. In *Pure and Applied Chemistry*; Butterworths: London, UK, 1972; pp. 579–638.
72. Barrett, E.P.; Joyner, L.G.; Halenda, P.P. The Determination of Pore Volume and Area Distributions in Porous Substances. I. Computations from Nitrogen Isotherms. *J. Am. Chem. Soc.* **1951**, *73*, 373–380. [CrossRef]
73. Wang, Q.; Luo, J.; Zhong, Z.; Borgna, A. CO_2 Capture by Solid Adsorbents and Their Applications: Current Status and New Trends. *Energy Environ. Sci.* **2011**, *4*, 42–55. [CrossRef]
74. Kundu, S.; Khandaker, T.; Anik, M.A.-A.M.; Hasan, M.K.; Dhar, P.K.; Dutta, S.K.; Latif, M.A.; Hossain, M.S. A Comprehensive Review of Enhanced CO_2 Capture Using Activated Carbon Derived from Biomass Feedstock. *RSC Adv.* **2024**, *14*, 29693–29736. [CrossRef]
75. Schneider, M.; Rodríguez-Castellón, E.; Guerrero-Pérez, M.O.; Hotza, D.; De Noni Junior, A.; de Fátima Peralta Muniz Moreira, R. Hierarchically Porous Composites Containing Mining Tailings-Based Geopolymer and Zeolite 13X: Application for Carbon Dioxide Sequestration. *Adsorption* **2025**, *31*, 21. [CrossRef]
76. Duxson, P.; Lukey, G.C.; van Deventer, J.S.J. Physical Evolution of Na-Geopolymer Derived from Metakaolin up to 1000 °C. *J. Mater. Sci.* **2007**, *42*, 3044–3054. [CrossRef]
77. He, R.; Dai, N.; Wang, Z. Thermal and Mechanical Properties of Geopolymers Exposed to High Temperature: A Literature Review. *Adv. Civ. Eng.* **2020**, *2020*, 7532703. [CrossRef]
78. Wang, R.; Meng, T.; Zhang, B.; Chen, C.; Li, D. Preparation and Characterization of Activated Carbon/Ultra-high Molecular Weight Polyethylene Composites. *Polym. Compos.* **2021**, *42*, 2728–2736. [CrossRef]

Disclaimer/Publisher's Note: The statements, opinions and data contained in all publications are solely those of the individual author(s) and contributor(s) and not of MDPI and/or the editor(s). MDPI and/or the editor(s) disclaim responsibility for any injury to people or property resulting from any ideas, methods, instructions or products referred to in the content.